Time-domain simulation of a guitar: Model and method[a)]

Grégoire Derveaux[b)]
INRIA Roquencourt, Projet Ondes, 78153 Le Chesnay Cedex, France

Antoine Chaigne[c)]
ENSTA, Chemin de la Hunière, 91761 Palaiseau Cedex, France

Patrick Joly and Eliane Bécache
INRIA Roquencourt, Projet Ondes, 78153 Le Chesnay Cedex, France

(Received 8 June 2003; revised 29 September 2003; accepted 3 October 2003)

This paper presents a three-dimensional time-domain numerical model of the vibration and acoustic radiation from a guitar. The model involves the transverse displacement of the string excited by a force pulse, the flexural motion of the soundboard, and the sound radiation. A specific spectral method is used for solving the Kirchhoff–Love's dynamic top plate model for a damped, heterogeneous orthotropic material. The air–plate interaction is solved with a fictitious domain method, and a conservative scheme is used for the time discretization. Frequency analysis is performed on the simulated sound pressure and plate velocity waveforms in order to evaluate quantitatively the transfer of energy through the various components of the coupled system: from the string to the soundboard and from the soundboard to the air. The effects of some structural changes in soundboard thickness and cavity volume on the produced sounds are presented and discussed. Simulations of the same guitar in three different cases are also performed: "*in vacuo*," in air with a perfectly rigid top plate, and in air with an elastic top plate. This allows comparisons between structural, acoustic, and structural–acoustic modes of the instrument. Finally, attention is paid to the evolution with time of the spatial pressure field. This shows, in particular, the complex evolution of the directivity pattern in the near field of the instrument, especially during the attack.
 [DOI: 10.1121/1.1629302]

PACS numbers: 43.75.Gh, 43.40.Rj [NHF] Pages: 3368–3383

I. INTRODUCTION

The scope of the reported study is the simulation of the three-dimensional sound-pressure field of a guitar in the time domain. In a guitar, the elastic waves in strings and soundboard, and the acoustic waves in both external air and cavity, are continuously evolving with time. Both fluid and structural waves interact continuously so that the system composed by the instrument, the cavity, and the surrounding air should be considered as a whole. This approach, which is essential for a good understanding of the time-varying vibroacoustical phenomena involved in a guitar, has been made possible by the use of advanced numerical methods.

The method used consists of modeling the vibratory and acoustical phenomena involved in the instrument from the initial pluck to the radiation in a three-dimensional space. Since we wish to focus on the modeling of the soundboard and on the fluid–structure interaction, the model used for the other parts of the instrument is intentionally kept simple. Thus, an idealized plucking force is acting on a one-dimensional damped string model. The motion of the string is assumed to be perpendicular to the top plate. The soundboard itself is more sophisticated, in order to account for its crucial role in the sound of a guitar. It is modeled as an orthotropic heterogeneous damped Kirchhoff–Love plate, with a hole, and clamped at its boundaries. The other constitutive parts of the guitar (back, sides, neck) are assumed to be rigid. These latter assumptions could be eventually revisited in future studies. The plate radiates both inside the cavity and in the external free field. The cavity communicates with the external field through the hole.

In its present state, the purpose of the work is to show the feasibility and the main principles of a complete guitar modeling. No comparison with a particular instrument has been made. The values of the various physical and geometrical parameters used in the simulations correspond to realistic values extracted from the existing literature on the guitar.

The complexity of the system makes it necessary to use different numerical techniques for solving the problem. The plate equation is solved with a specific spectral method. A fictitious domain method, similar to the one previously used by Rhaouti *et al.* for timpani, is used for solving the fluid–structure interaction.[1] Finally, a conservative scheme is used for the time discretization.

The paper starts with the presentation of the guitar model, which is followed by the numerical formulation of the problem. The fourth section is devoted to the presentation of selected preliminary results whose aim is to show the

[a)]Preliminary results to the present study were first reported at: Forum Acusticum, Séville, Spain (*Time-domain simulation of a guitar: Preliminary results*, Forum Acusticum 2002, Special Issue of the Revista de Acustica, Vol. 33) and 144th Acoustical Society of America Meeting, Cancun, Mexico ["Time-domain simulation of a guitar," J. Acoust. Soc. Am. **112**, 2409 (2002)]. The numerical aspects of the method were presented at the Second M.I.T. Conference on Computational Fluid and Solid Mechanics (June, 2003).

[b)]Present address: ENSTA-UMA, 32 Bd Victor, 75015 Paris, France.
[c)]Electronic mail: chaigne@ensta.fr

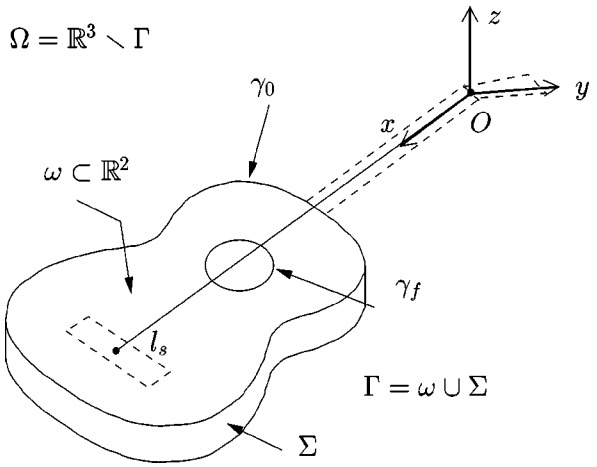

FIG. 1. Geometrical description of the guitar.

main attributes of the method. The detailed presentation of the application of the model to important features in the context of guitar acoustics, such as sound power and efficiency, is left for future studies.

With regard to previous work on guitars, one can summarize the originality of the present work as follows: First, the cavity model and the air–structural coupling is more general than in the boundary element method, developed by Richardson *et al.*[2] It is also a step forward compared to the spatial Fourier method developed by Le Pichon *et al.*, where the velocity distribution on the surface of the body was measured, and not calculated.[3] Second, the results obtained in the time domain with the present model should be compared to the results obtained in the frequency domain by Elejabarrieta *et al.*, who used commercial software.[4] In particular, the bracing used in our model is less accurate than in this latter paper. However, more emphasis is put here on the description of the air sound field and on the effects of the pressure jump on the top plate.

Finally, as far as the numerical technique is concerned, the present modeling is a direct extension to plates of the timpani model developed by Rhaouti *et al.*[1] The modeling of damping in the guitar top plate makes use also of results obtained by Chaigne and Lambourg.[5]

II. PRESENTATION OF THE MODEL

A. Description

The body of the guitar is delimited by a surface denoted Γ which is divided into two parts: $\Gamma = \omega \cup \Sigma$, where ω is the top plate of the instrument and Σ is the rest of the surface (i.e., sides and back). The boundary of ω itself is divided into two parts: γ_0 is the outer boundary of the top plate and γ_f is the inner boundary, along the hole. The surrounding air occupies the domain $\Omega = \mathbb{R}^3 \setminus \Gamma$. Ω corresponds to the internal cavity and the external domain, which communicate via the sound hole. The string of length l_s is rigidly fixed to the neck at a point denoted O, chosen as the origin of the coordinate system (see Fig. 1).

B. The string

The string is supposed to have uniform density ρ_s, uniform tension T, and no stiffness. In the following, only the vertical flexural motion of the soundboard will be considered. Therefore, it is also natural to consider only the vertical polarization of the string. The motion of the string is thus described by its transverse displacement (perpendicular to the soundboard) denoted $u_s(x,t)$, $x \in]0,l_s[$. Assuming that the amplitudes of vibration are sufficiently small, the string equation is a classical 1D damped wave equation

$$\rho_s \frac{\partial^2 u_s}{\partial t^2} - T\left(1 + \eta_s \frac{\partial}{\partial t}\right)\frac{\partial^2 u_s}{\partial x^2} + \rho_s R_s \frac{\partial u_s}{\partial t} = f_s(x,t), \quad \text{in }]0,l_s[. \tag{1}$$

The internal damping is modeled by two terms: a viscoelastic term with coefficient η_s whose essential purpose is to introduce a frequency-dependent damping in the string, and a fluid term with coefficient R_s whose purpose is to introduce a constant internal damping for low frequencies. The string is fixed at one end to the neck of the guitar, which is supposed to be perfectly rigid

$$u_s(0,t) = 0, \quad \forall t > 0. \tag{2}$$

At the bridge, the displacement of the string is assumed to be given by the displacement of the plate at the contact point between string and bridge, denoted (x_0, y_0)

$$u_s(l_s,t) = u_p(x_0,y_0,t), \quad \forall t > 0. \tag{3}$$

The plucking of the string is assumed to be an imposed force (see Fig. 2 and Table I)

$$f_s(x,t) = g(x)h(t), \tag{4}$$

where $h(t)$ represents a simple idealized version of the ''stick–slip'' mechanism that governs the interaction between string and finger. One pulls on the string during nearly

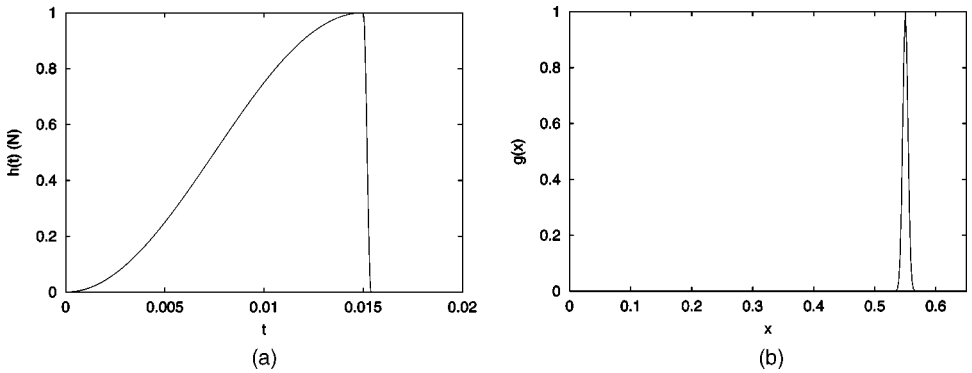

FIG. 2. Representation of the idealized plucking force. (a) Time dependence. (b) Space dependence.

TABLE I. Typical values of physical and numerical values used for the simulations.

String: $\rho_s = 0.005\,25\ \mathrm{kg\cdot m^{-1}}$, $T = 60$ N, $l_s = 0.65$ m,
$R_s = 0.75\ \mathrm{s^{-1}}$, $\eta_s = 9\cdot 10^{-8}$ s, $(x_0, y_0) = (65\ \mathrm{cm}, 4\ \mathrm{cm})$

Soundboard:

	D_1 (MPa)	D_2 (MPa)	D_3 (MPa)	D_4 (MPa)	ρ_p ($\mathrm{kg\cdot m^{-1}}$)	a (mm)	R_p ($\mathrm{s^{-1}}$)	η_p (s)
Plate	850	50	75	200	350	2.9	7	0.005
Bridge	80	50	900	270	400	6	7	0.005
Struts	100	60	1250	300	400	14	7	0.005

Air: $c_a = 344\ \mathrm{m\cdot s^{-1}}$, $\rho_a = 1.21\ \mathrm{kg\cdot m^{-3}}$

Numerical information:

String:	308 nodes	$h_c = 2.1$ mm
Plate:	3230 nodes	$h_p = 1.2$ cm
Pressure jump:	1260 nodes	$h_\lambda = 1.2$ cm
Acoustic field:	≈400 000 cubes	$h_a = 1.1$ cm
Time step:	$\Delta t = 2.10^{-5}$ s	
Sampling frequency:	$f_e = 50\,000$ Hz	

Plucking force: $f_s(x,t) = g(x)h(t)$.

$$g(x) = \frac{\exp(-(x-x_0/\delta_s)^2)}{\int_0^{l_s}\exp(-(x-x_0/\delta_s)^2)} \qquad h(t) = \begin{cases} (1-\cos(\pi t/t_1)), & 0 \leqslant t \leqslant t_1, \\ (1+\cos(\pi(t-t_1)/t_2)), & t_1 \leqslant t \leqslant t_2, \\ 0, & t > t_2. \end{cases}$$

$x_0 = 55$ cm, $\delta_c = 0.006$ m, $t_1 = 0.015$ s, $t_2 = 0.000\,4$ s.

15 ms and releases it during 0.4 ms. This force is distributed over a small segment of the string by means of the smooth positive function g, normalized so that $\int_0^{l_s} g(x)dx = 1$. Despite its simplicity, this excitation is in fairly good agreement with experiments.[6]

C. The soundboard

It is assumed that the only vibrating part of the guitar is the soundboard. The other parts of the guitar body (back, sides, neck) are assumed to be perfectly rigid. If necessary, the motion of the back could be introduced straightaway in this model since it is of exactly the same nature as the top plate. The soundboard is a thin, orthotropic wooden layer, with a soundhole. The thickness is relatively small (about 3 mm) compared to the dimensions of the soundboard (about 50 cm long). In terms of spectral content, our study is limited to the bandwidth 0–3000 Hz. For both these reasons, it is not necessary to use a thick plate model, such as the Reissner–Mindlin one. The flexural Kirchhoff–Love's plate model is thus appropriate to describe the vibrations of the soundboard.

The strutting system and the bridge are considered as heterogeneities of the soundboard. As a consequence, the following physical parameters which characterize the top plate are variable functions of space: density $\rho_p(x,y)$, thickness $a(x,y)$, and rigidity tensor for orthotropic material $\mathbf{C}(x,y)$. In what follows, the space dependence of these parameters will be omitted, in order to simplify the notations.

Finally, the in-plane motion of the soundboard is neglected compared to its flexural motion. The motion of the strutted soundboard is thus completely described by the transverse displacement of the top plate, denoted $u_p(x,y,t)$, $(x,y) \in \omega$. This motion is governed by the following equation:[7–10]

$$a\rho_p \frac{\partial^2 u_p}{\partial t^2} + \left(1 + \eta_p \frac{\partial}{\partial t}\right) \mathrm{div}\,\underline{\mathrm{Div}}\; a^3 \mathbf{C}\underline{\underline{\varepsilon}}(\underline{\nabla} u_p) + a\rho_p R_p \frac{\partial u_p}{\partial t} = \mathcal{F} - [p]_\omega, \quad \text{in } \omega, \tag{5}$$

where $\underline{\mathrm{Div}}$ is the divergence operator for tensors: $(\underline{\mathrm{Div}}.\tau) = \partial_j \tau_{ij}$, $\underline{\underline{\varepsilon}}$ is the plane linearized strain tensor $[\varepsilon_{\alpha\beta}(\underline{\theta}) = \frac{1}{2}(\partial_\beta \theta_\alpha + \partial_\alpha \theta_\beta)]$, div and $\underline{\nabla}$ denote the usual divergence operator and gradient operator for vectors, respectively (see Appendix A for details and more explicit notations).

As for the string, the internal damping in the plate is modeled by two terms: a viscoelastic term with coefficient η_p and a fluid term with coefficient R_p. Notice, however, that since a spectral method is used for the numerical resolution of this equation, it becomes possible to introduce other laws of damping, which do not need to have so simple a counterpart in the time domain. This point will be developed in Sec. III C.

The top plate is clamped on γ_0

$$u_p = 0 \quad \text{and} \quad \partial_n u_p = 0, \quad \text{on} \quad \gamma_0, \tag{6}$$

whereas the boundary is free along the hole γ_f (see Appendix A for explicit notations in particular cases)

$$\begin{aligned} &(\underline{\underline{\mathcal{M}}}\,\underline{n}) \cdot \underline{n} = 0, \quad \text{on} \quad \gamma_f, \\ &(\underline{\mathrm{Div}}\,\underline{\underline{\mathcal{M}}}) \cdot \underline{n} + \partial_\tau[(\underline{\underline{\mathcal{M}}}\,\underline{n}) \cdot \underline{\tau}] = 0, \quad \text{on} \quad \gamma_f, \end{aligned} \tag{7}$$

where $\underline{\underline{\mathcal{M}}} = a^3 \mathbf{C}\underline{\underline{\varepsilon}}(\underline{\nabla} u_p)$ is the bending moment. $\underline{n}$ denotes the outer normal and $\underline{\tau}$ the tangential vector along the boundary γ_f. The two conditions in Eq. (7) express approximately that force and moment vanish at the free boundary.

The force density term exerted on the plate by the surrounding air is $[p]_\omega$, the pressure jump across the soundboard. $\mathcal{F}$ denotes the force density exerted by the string on the bridge. It is assumed to be the normal component of the

tension of the string at this point. This force is applied at the contact point (x_0,y_0) between string and bridge

$$\mathcal{F}(x,y,t)\approx -T\partial_x u_s(l_s,t)\,\delta_{x_0,y_0}(x,y). \tag{8}$$

D. The acoustic field

The acoustic field is governed by the linearized Euler's equations

$$\frac{\partial p}{\partial t}=-c_a^2\rho_a\,\mathrm{div}(\underline{\mathbf{v}}_a) \quad \text{in } \Omega, \tag{9a}$$

$$\rho_a\frac{\partial \underline{\mathbf{v}}_a}{\partial t}=-\underline{\nabla}p \quad \text{in } \Omega, \tag{9b}$$

where c_a is the speed of the sound in air, ρ_a is the density of air, p is the sound pressure in Ω, and $\underline{\mathbf{v}}_a$ the acoustic velocity in Ω. These equations are complemented by a condition of continuity for the normal component of the velocity at the surface ω of the plate

$$\underline{\mathbf{v}}_a(x,y,0,t)\cdot\mathbf{e}_z=\partial_t u_p(x,y,t), \quad \forall (x,y)\in\omega, \quad \forall t>0. \tag{10}$$

In addition, as the body of the guitar is assumed to be perfectly rigid, one has

$$\underline{\mathbf{v}}_a(x,y,z,t)\cdot\mathbf{N}_\Gamma=0, \quad \forall (x,y,z)\in\Gamma, \quad \forall t>0, \tag{11}$$

where $\mathbf{N}_\Gamma$ denotes the outer normal to the boundary Σ.

E. Energy decay

The system of coupled equations (1) to (11) fulfills a property of energy decay in the case of free oscillations. The respective energies of the string E^s, plate E^p, and sound field E^a, are given by

$$\begin{aligned}
E^s(t)&=\frac{1}{2}\int_0^{l_s}\rho_s\left|\frac{du_s}{dt}\right|^2dx+\frac{1}{2}\int_0^{l_s}T\left|\frac{du_s}{dx}\right|^2dx,\\
E^p(t)&=\frac{1}{2}\int\int_\omega \rho_p a\left|\frac{du_p}{dt}\right|^2dx\,dy\\
&\quad+\frac{1}{2}\int\int_\omega a^3\mathbf{C}\underline{\underline{\varepsilon}}(\underline{\nabla}u_p):\underline{\underline{\varepsilon}}(\underline{\nabla}u_p)dx\,dy,\\
E^a(t)&=\frac{1}{2}\int\int\int_\Omega \rho_a|\underline{\mathbf{v}}_a|^2dx\,dy\,dz\\
&\quad+\frac{1}{2}\int\int\int_\Omega\frac{1}{c_a^2\rho_a}|p|^2dx\,dy\,dz.
\end{aligned} \tag{12}$$

It is easy to show that the total energy of the system $E=E^s+E^p+E^a$ fulfills the following identity property:

$$\begin{aligned}
\frac{dE}{dt}(t)&=\int_0^{l_s}f_s\frac{du_s}{dt}dx-\int_0^{l_s}\eta_s T|\partial_{x,t}u_s|^2dx\\
&\quad-\int_0^{l_s}\rho_s R_s|\partial_t u_s|^2dx\\
&\quad-\int\int_\omega \eta_p a^3\mathbf{C}\underline{\underline{\varepsilon}}(\underline{\nabla}\partial_t u_p):\underline{\underline{\varepsilon}}(\underline{\nabla}\partial_t u_p)dx\,dy\\
&\quad-\int\int_\omega a\rho_p R_p|\partial_t u_p|^2dx\,dy.
\end{aligned} \tag{13}$$

In addition to its physical meaning, this property guarantees the wellposedness of the continuous model and will be exploited for ensuring the stability of the numerical scheme, as it will be shown in the next section.

III. NUMERICAL RESOLUTION

Let us begin with a brief description of the main difficulties we have to face in order to solve these equations numerically. The 3D nature of the computational domain for the sound radiation yields a large size problem. This domain is unbounded, so that it is necessary to reduce it to a finite size problem, in order to make it computable. The geometry of the instrument is complex and includes third-order boundary conditions [Eq. (7)]. Furthermore, the space- and time discretization of the Kirchhoff–Love equation requires an adapted resolution method, because this equation includes a fourth-order space operator and is intrinsically dispersive. Last but not least, one has to derive a stable resolution scheme.

The problem is first rewritten as an equivalent variational formulation, which is the first step of the finite element method. A variational formulation corresponds to the virtual work principle which is naturally related to the continuous energy identity [Eq. (13)]. The conforming space approximation of the variational formulation of the problem leads to a discrete energy identity, which is a convenient approach to derive the stability of the resolution scheme. The main aspects of the numerical resolution are the following:

(i) The plate equation is solved by a modal decomposition method (Secs. III A 1 and III C).
(ii) The fluid–structure interaction problem is solved with the use of the fictitious domain method (Sec. III A 2).
(iii) One of the main originalities of the method is a stable coupling between a continuous time resolution and a discrete one (Sec. III C).

In what follows, for the sake of simplicity, the damping in the plate is described by a single fluid damping term, and there is no damping in the string. It does not add formal difficulty to take into account the other damping terms presented in Eqs. (1) and (5).

A. Variational formulation

1. The plate

A well-known difficulty for the resolution of the Kirchhoff–Love's problem is due to the presence of a fourth-order space operator. This operator would require *a priori* the use of sophisticated finite elements of class C^1, with continuity of the normal derivative along each edge of the plate triangulation. To circumvent this difficulty, the space operator is split into two second-order operators. We introduce the velocity $v_p=\partial_t u_p$ and the bending moment $\underline{\underline{\mathcal{M}}}=\underline{\underline{\varepsilon}}(\underline{\nabla}u_p)$, which leads to the following equivalent problem of second order in space and first order in time:

$$a\rho_p \partial_t v_p + \operatorname{div} \underline{\operatorname{Div}} \underline{\underline{\mathcal{M}}} + a\rho_p R_p v_p = \mathcal{F} - [p]_\omega, \quad \text{in } \omega, \tag{14a}$$

$$\partial_t \underline{\underline{\mathcal{M}}} - a^3 \mathbf{C} \underline{\underline{\varepsilon}}(\underline{\nabla} v_p) = 0, \quad \text{in } \omega, \tag{14b}$$

$$v_p = \partial_n v_p = 0, \quad \text{on } \gamma_0, \tag{14c}$$

to which the conditions on the free boundary given by Eq. (7) are added. The variational formulation of Eq. (14) is obtained by multiplying Eq. (14a) by a test function $v_p^* : \omega \to \mathbb{R}$ and by multiplying equation Eq. (14b) by a test function $\underline{\underline{\mathcal{M}}}^* : \omega \to \mathbb{R}^4$. Using then an integration by parts on ω leads to the following mixed formulation:

Find $v_p(t) : \omega \to \mathbb{R}$ and $\underline{\underline{\mathcal{M}}}(t) : \omega \to \mathbb{R}^4$ such that

$$\frac{d}{dt} \int_\omega a\rho_p v_p v_p^* - \int_\omega \underline{\operatorname{Div}} \underline{\underline{\mathcal{M}}} \cdot \underline{\nabla} v_p^* - \int_{\gamma_f} \partial_\tau [(\underline{\underline{\mathcal{M}}} \underline{n}) \cdot \underline{\tau}] v_p^* + \int_\omega a\rho_p R_p v_p v_p^* = -T \partial_x u_s(l_s, t) v_p^*(x_0, y_0) - \int_\omega [p]_\omega v_p^*, \quad \forall v_p^*, \tag{15a}$$

$$\frac{d}{dt} \int_\omega a^{-3} \mathbf{C}^{-1} \underline{\underline{\mathcal{M}}} : \underline{\underline{\mathcal{M}}}^* + \int_\omega \underline{\operatorname{Div}} \underline{\underline{\mathcal{M}}}^* \cdot \underline{\nabla} v_p + \int_{\gamma_f} \partial_\tau [(\underline{\underline{\mathcal{M}}}^* \underline{n}) \cdot \underline{\tau}] v_p = 0, \quad \forall \underline{\underline{\mathcal{M}}}^*. \tag{15b}$$

The main interest of this formulation is that it can be approximated using standard Lagrange finite elements (see Sec. III B).

2. The fluid–structure interaction

With regards to the large size of the problem, the finite difference method would certainly be an efficient approach for solving the acoustic equation in terms of computational time, since it relies on the use of a regular mesh made of small cubes. Unfortunately, this choice leads to a staircase approximation of the complex geometry of the guitar which generates spurious diffractions.[11] Furthermore, the construction of a coupling scheme with the finite element method used for the plate problem is not straightforward because of the incompatibility of the meshes. As an alternative, the finite element method allows one to take into account the shape of the instrument accurately. However, this method requires the construction of a tetrahedric mesh and leads to a quite expensive resolution scheme, with regard to computing time and memory.

In practice, we used a fictitious domain method, first introduced by Glowinsky,[12] and which has been successfully applied to kettledrums by Rhaouti *et al.*[1] The fictitious domain method preserves the advantages of both previously mentioned methods: the efficiency of the finite difference method in terms of computing time, and the good approximation of the shape of the guitar. Its leading idea is to reformulate the problem in a domain of simple geometry which ignores the instrument. The fluid–structure interaction is then taken into account via the introduction of the new unknown variable $\lambda = [p]_\Gamma = p_e - p_i$, defined on Γ which denotes the pressure jump across the boundary of the instrument.

Multiplying Eq. (9a) by a test function $p^* : \mathbb{R}^3 \to \mathbb{R}$, and Eq. (9b) by a test function $\underline{\mathbf{v}}_a^* : \mathbb{R}^3 \to \mathbb{R}^3$, and using the Green formula leads to Eqs. (16a) and (16b). It remains to take into account the boundary conditions given by Eqs. (10) and (11) on the surface of the instrument, which is done in a weak sense [Eq. 16(c)]. This leads to the following problem:

Find $p(t) : \mathbb{R}^3 \to \mathbb{R}$, $\underline{\mathbf{v}}_a(t) :: \mathbb{R}^3 \to \mathbb{R}^3$, and $\lambda(t) : \Gamma \to \mathbb{R}$ such that

$$\frac{d}{dt} \int_{\mathbb{R}^3} \frac{1}{\rho_a c_a^2} p p^* + \int_{\mathbb{R}^3} p^* \operatorname{div} \underline{\mathbf{v}}_a = 0, \quad \forall p^*, \tag{16a}$$

$$\frac{d}{dt} \int_{\mathbb{R}^3} \rho_a \underline{\mathbf{v}}_a \cdot \underline{\mathbf{v}}_a^* - \int_{\mathbb{R}^3} p \operatorname{div} \underline{\mathbf{v}}_a^* - \int_\Gamma (\underline{\mathbf{v}}_a^* \cdot \underline{N}) \lambda = 0, \quad \forall \underline{\mathbf{v}}_a^*, \tag{16b}$$

$$\int_\omega v_p \lambda^* - \int_\Gamma (\underline{\mathbf{v}}_a \cdot \underline{N}) \lambda^* = 0, \quad \forall \lambda^*. \tag{16c}$$

In Eq. (16), $\underline{\mathbf{v}}_a$ and p are defined in the complete domain $\mathbb{R}^3$, and not only in the domain $\Omega = \mathbb{R}^3 \backslash \Gamma$. It will then be possible to use a regular mesh for the approximation of the acoustic field. It turns out that this choice leads in fact to a finite difference scheme, which is the major interest of the fictitious domain method. In addition, the geometry of the instrument is well fitted, since it relies on a triangular mesh of its surface for the approximation of λ, which is easy to construct.

3. The string

Because the plate velocity v_p has been introduced in order to solve the Kirchhoff–Love's problem [Eq. (14)], one has to differentiate in time the boundary condition at the bridge given by Eq. (3). This leads naturally to introduce the string velocity $v_s = \partial_t u_s$. It can be shown that in order to preserve the energy identity [Eq. (13)], one also has to introduce the constraint $q = T \partial_x u_s$, which appears, in particular, in the expression of the force exerted by the string on the plate [Eq. (8)]. The following problem of first order in space and first order in time is obtained:

$$\begin{aligned} &\rho_s \partial_t v_s - \partial_x q = f_s, \quad \text{in }]0, l_s[\\ &\partial_t q - T \partial_x v_s = 0, \quad \text{in } 0, l_s[\\ &v_s(0,t) = 0, \quad \forall t \\ &v_s(l_s, t) = v_p(x_0, y_0), \quad \forall t. \end{aligned} \tag{17}$$

The variational formulation of Eq. (17) is obtained by multiplying the first equation by a test function $v_s^* :]0, l_s[\to \mathbb{R}$, and the second by a test function $q^* :]0, l_s[\to \mathbb{R}$, and using integration by part. This leads to the following problem:

Find $v_s : [0, l_s[\to \mathbb{R}$ and $q :]0, l_s[\to \mathbb{R}$ such that

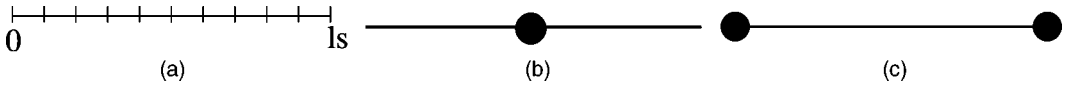

FIG. 3. Mesh for (v_{s_h}, q_h). (a) Mesh of $]0, l_s[$. (b) Degrees of freedom for v_s. (c) Degrees of freedom for q.

$$\frac{d}{dt}\int_0^{l_s} \rho_s v_s v_s^* - \int_0^{l_s} \partial_x q v_s^* = \int_0^{l_s} f_s v_s^*, \quad \forall v_s^*, \tag{18a}$$

$$\frac{d}{dt}\int_0^{l_s} \frac{1}{T} q q^* + \int_0^{l_s} \partial_x q^* v_s - q^*(l_s,t) v_p(x_0,y_0) = 0, \quad \forall q^* \tag{18b}$$

4. Variational formulation of the complete problem

Considering the additional unknowns λ and q, which were introduced in order to solve the acoustic equation and the string equation, respectively, one has to replace $T\partial_x u_s(l_s,t)$ by $q(l_s,t)$ and $[p]_\omega$ by $\lambda_{|\omega}$ in Eq. (15a). Equation (15a) is thus replaced by

$$\frac{d}{dt}\int_\omega \rho_p v_p v_p^* - \int_\omega \underline{\mathrm{Div}}\underline{\underline{\mathcal{M}}} \cdot \underline{\nabla} v_p^* - \int_{\gamma_f} \partial_\tau[(\underline{\underline{\mathcal{M}}}\underline{n}) \cdot \underline{\tau}] v_p^* + \int_\omega \rho_p R_p v_p v_p^* = -q(l_s,t) v_p^*(x_0,y_0) - \int_\omega \lambda_{|\omega} v_p^*, \quad \forall v_p^* : \omega \to \mathbb{R}. \tag{19}$$

Finally, the variational formulation of the complete problem is given by the set of equations (15b), (16), (18), (19).

B. Space discretization

In this variational formulation, the unknowns $(v_s, q, v_p, \underline{\underline{\mathcal{M}}}, p, \underline{\mathbf{v}}_a, \lambda)$ and the test functions $(v_s^*, q^*, v_p^*, \underline{\underline{\mathcal{M}}}^*, p^*, \underline{\mathbf{v}}_a^*, \lambda^*)$ are chosen in appropriate spaces so that all integrals are defined. q has to be chosen in a space of continuous functions because of the term $\partial_x q$ in Eq. (18). For similar reasons, v_p, $\underline{\underline{\mathcal{M}}}$, and λ will also be chosen in a space of continuous functions. On the other hand, the spaces for v_s and for p do not require any condition of continuity. Finally, $\underline{\mathbf{v}}_a$ is in a space of vector field with continuity of the normal component across the surface, because of the term $\mathrm{div}\,\underline{\mathbf{v}}_a$ in Eq. (16).

The finite dimensional spaces chosen for the approximation of the variational formulation (15b), (16), (18), (19) and satisfying the adequate continuity conditions are described below. In the following P_k denotes the polynomial functions of one or more variables of degree less than or equal to k.

The continuous variables v_s and q are approximated by discrete variables in space denoted v_{s_h} and q_h, respectively. A regular mesh of the string, made of small segments of length h_c is constructed [Fig. 3(a)]. v_{s_h} is a piecewise constant and is thus entirely determined by its values at the center of each segment, which are called the degrees of freedom (dof). In other words v_{s_h} is discretized using P_0 discontinuous finite elements. q_h is a continuous piecewise linear function and it is thus fully determined by its values at each node of the mesh (P_1 continuous finite elements). The degrees of freedom for v_{s_h} and q_h are represented in Figs. 3(b) and (c), respectively.

Given a triangular mesh of the soundboard ω, with the smallest edge length denoted h_p [Fig. 4(a)], the variables v_p and $\underline{\underline{\mathcal{M}}}$ are discretized by means of P_2 alike-continuous finite elements.[13] This particular choice reduces the numerical dispersion and leads to the required estimation of the eigenfrequencies of the soundboard.[13] With regard to sound synthesis it is an important aim to simulate the eigenfrequencies of the soundboard with sufficient accuracy, in view of the ability of the human ear to detect small frequency variations. In this context, an order of magnitude of 1% seems a reasonable target. An analysis of the performance of finite element approximations of different orders for the plate equation is presented in Appendix B. Another advantage of using P_2 elements lies in the elimination of the unknown $\underline{\underline{\mathcal{M}}}_h$ in the final scheme, as it will be shown in Sec. III C.

The discrete variables v_{p_h} and $\underline{\underline{\mathcal{M}}}_h$ are determined by their values at the vertex, at the gravity center of each triangle, and at the center of each edge. The degrees of freedom for v_{p_h} and $\underline{\underline{\mathcal{M}}}_h$ are represented in Figs. 4(b) and (c), respectively.

To simulate the free space, the computations are restricted to a box of finite size denoted $\mathcal{C}$, with the help of higher-order absorbing boundary conditions defined on the faces of this cube.[1,14] For the sake of conciseness, these additional equations $\mathcal{C}$ are not given here. Given a regular mesh of $\mathcal{C}$, made of small cubes with edge length denoted h_a [Fig. 5(a)], p is discretized by means of P_0-discontinuous finite

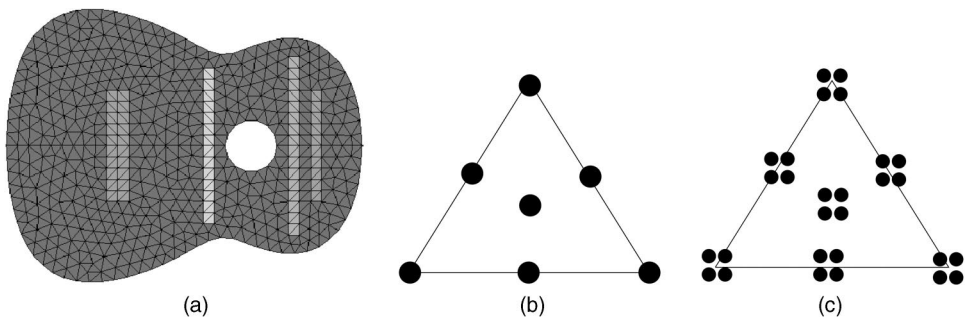

FIG. 4. Mesh for $(v_{p_h}, \underline{\underline{\mathcal{M}}}_h)$. (a) Mesh of ω. (b) Degrees of freedom for v_{p_h}. (c) Degrees of freedom for $\underline{\underline{\mathcal{M}}}_h$.

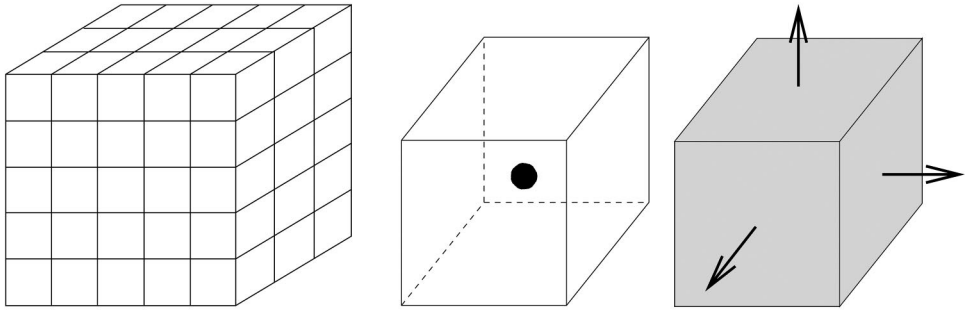

FIG. 5. Mesh for $(p_h, \underline{\mathbf{v}}_{a_h})$. (a) Mesh of $\mathcal{C}$. (b) Degrees of freedom for p_h. (c) Degrees of freedom for $\underline{\mathbf{v}}_{a_h}$.

elements. The field p_h is thus determined by its values at the center of each cube. The approximation of $\underline{\mathbf{v}}_a$ is made with the first-order Raviart–Thomas finite element space.[15] Each component of $\underline{\mathbf{v}}_{a_h}$ is linear in one direction and constant in the other two directions. $\underline{\mathbf{v}}_{a_h}$ is entirely determined by the value of its normal component across each face of the cubes. The degrees of freedom for p_h and $\underline{\mathbf{v}}_{a_h}$ are represented in Figs. 5(b) and (c), respectively.

Finally, a triangular mesh is given on the surface of the guitar Γ, with the smallest edge length denoted h_λ [see Fig. 6(a)]. The pressure jump λ is discretized by means of P_1 continuous finite elements. Its approximation λ_h is determined by the values at the vertex of each triangle. The degrees of freedom of λ_h are represented in Fig. 6(b).

The space discretization of the problem is then obtained by substituting $(v_{s_h}, q_h, v_{p_h}, \underline{\underline{\mathcal{M}}}_h, p_h, \underline{\mathbf{v}}_{a_h}, \lambda_h)$ for $(v_s, q, v_p, \underline{\underline{\mathcal{M}}}, p, \underline{\mathbf{v}}_a, \lambda)$ and $(v_{s_h}^*, q_h^*, v_{p_h}^*, \underline{\underline{\mathcal{M}}}_h^*, p_h^*, \underline{\mathbf{v}}_{a_h}^*, \lambda_h^*)$ for $(v_s^*, q^*, v_p^*, \underline{\underline{\mathcal{M}}}^*, p^*, \underline{\mathbf{v}}_a^*, \lambda^*)$ in the variational formulation (15b), (16), (18), (19). The resulting differential system can be written in the following matrix form:

$$M_h^p \frac{dv_{p_h}}{dt} - H_h^{\mathsf{T}} \underline{\underline{\mathcal{M}}}_h + R_p M_h^p v_{p_h} = -J_h q_h - (B_{\omega_h})^{\mathsf{T}} \lambda_h, \tag{20a}$$

$$M_h^{\mathcal{M}} \frac{d\underline{\underline{\mathcal{M}}}_h}{dt} + H_h v_{p_h} = 0, \tag{20b}$$

$$M_h^s \frac{dv_{s_h}}{dt} - D_h q_h = f_{s_h}, \tag{20c}$$

$$M_h^q \frac{dq_h}{dt} + D_h^{\mathsf{T}} v_{s_h} - J_h^{\mathsf{T}} v_{p_h} = 0, \tag{20d}$$

$$M_h^a \frac{d\underline{\mathbf{v}}_{a_h}}{dt} - G_h p_h - (B_{\Gamma_h})^{\mathsf{T}} \lambda_h = 0, \tag{20e}$$

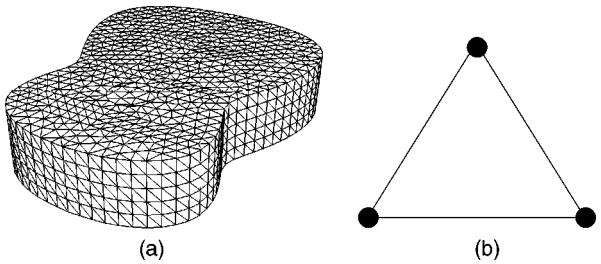

FIG. 6. Mesh for λ_h. (a) Mesh of Γ. (b) Degrees of freedom for λ_h.

$$M_h^{p_a} \frac{dp_h}{dt} + G_h^{\mathsf{T}} \underline{\mathbf{v}}_{a_h} = 0, \tag{20f}$$

$$B_{\omega_h} v_{p_h} - B_{\Gamma_h} \underline{\mathbf{v}}_{a_h} = 0, \tag{20g}$$

where A_h^{T} denotes the transpose of a matrix A_h. M_h^s, M_h^q, $M_h^{\mathcal{M}}$, M_h^a, and $M_h^{p_a}$ are mass matrices. f_{s_h} denotes a vector which approximates the plucking force exerted on the string. D_h, J_h, H_h, C_h, B_{ω_h}, G_h, and B_{Γ_h} are matrices which represent the discrete operators approximating the continuous operators of the variational formulation (15b), (16), (18), (19). G_h, for example, is the approximation of the three-dimensional gradient operator $\underline{\nabla}$.

C. Time discretization

For the time discretization, a classical explicit centered finite difference scheme of second order is used for the string and for the acoustic field. For the plate equation, it appears that the choice of an explicit finite difference scheme in time imposes the selection of a small time step Δt because of a restricting stability condition of the form $\Delta t \leqslant C h_p^2$, where C is a constant depending on the physical parameters of the plate. A natural idea would be to choose an implicit, unconditionally stable scheme, allowing a larger Δt. However, in this case the analysis of the error made on the eigenfrequencies of the soundboard shows that, for accuracy considerations, one has to choose Δt proportional to h_p^2 as for the explicit scheme.[16] For this reason, it has been finally decided to solve the plate equation analytically in time, which allows one to choose Δt without degrading the accuracy of the semidiscretized spatial scheme.

In a first step, the size of the plate system is reduced by eliminating the bending moment $\underline{\underline{\mathcal{M}}}_h$ in Eqs. (20a) and (20b), which leads to

$$M_h^p \frac{d^2 v_{p_h}}{dt^2} + R_p M_h^p \frac{dv_{p_h}}{dt} + K_h v_{p_h} = -J_h \frac{dq_h}{dt} - B_{\omega_h}^{\mathsf{T}} \frac{d\lambda_h}{dt}, \quad \forall t \geqslant 0, \tag{21}$$

where K_h is the matrix defined by

$$K_h = H_h (M_h^{\mathcal{M}})^{-1} H_h^{\mathsf{T}}. \tag{22}$$

The matrix $M_h^{\mathcal{M}}$ is computed using quadrature formula so that it reduces to a 4×4 block diagonal matrix, without loss of accuracy. This technique, called mass lumping, permits

one to invert $M_h^{\mathcal{M}}$, and, consequently, permits one to compute K_h easily.[13]

For the resolution of Eq. (21), one has to sample the solution. Given a time step Δt, v_{p_h} and $\dot{v}_{p_h}=dv_{ph}/dt$ are calculated at the successive instants of time $t^{n+(1/2)}=(n+\frac{1}{2})\Delta t$. Equation (21) is solved on each interval $[t^{n-(1/2)},t^{n+(1/2)}]$. Since the string and acoustic equations of the problem are solved by means of finite differences with time step Δt, the right-hand side is constant on this interval. The following equation is thus solved at each time step:

$$M_h^p\frac{d^2v_{p_h}}{dt^2}+R_pM_h^p\frac{dv_{p_h}}{dt}+K_hv_{p_h}=-J_h\frac{q_h^{n+1}-q^{n-1}}{2\Delta t}-B_{\omega_h}^{\mathsf{T}}\frac{\lambda_h^{n+(1/2)}-\lambda_h^{n-(1/2)}}{\Delta t},\quad \forall t\in\,]t^{n-(1/2)},t^{n+(1/2)}[,$$

$$v_{p_h}(t^{n-(1/2)})=v_{p_h}^{n-(1/2)}\ \text{ and }\ \dot{v}_{p_h}(t^{n-(1/2)})=\dot{v}_{p_h}^{n-(1/2)}. \tag{23}$$

The resolution of Eq. (23) relies on the computation of the eigenmodes of the positive definite matrix K_h, and on the ordinary differential equation theory. In the absence of damping, the solution is given by

$$v_{p_h}^{n+(1/2)}=\left[\cos(\sqrt{K_h}\Delta t)v_{p_h}^{n-(1/2)}+\frac{\sin(\sqrt{K_h}\Delta t)}{\sqrt{K_h}}\dot{v}_{p_h}^{n-(1/2)}\right]+\frac{I-\cos(\sqrt{K_h}\Delta t)}{\sqrt{K_h}}\left(-J_h\frac{q_h^{n+1}-q^{n-1}}{2\Delta t}-B_{\omega_h}^{\mathsf{T}}\frac{\lambda_h^{n+(1/2)}-\lambda_h^{n-(1/2)}}{\Delta t}\right), \tag{24}$$

with a similar equation for $\dot{v}_{p_h}^{n+(1/2)}$. For our computations, only the first 50 modes of the plate were retained, which corresponds to a cutoff frequency nearly equal to 3 kHz.

The introduction of the damping terms leads in fact to exponentially damped sinusoidal solutions for each modal component. It is a well-known fact that the fluid and viscoelastic terms introduced in the model [R_p and η_p in Eq. (5)] lead to a damping factor $\alpha_n=(R_p+\eta_p\omega_n^2)/2$ for the nth eigenmode of K_h with pulsation ω_n. At this stage, notice that it is possible to choose any other frequency dependence for the damping factors, without requiring that it has a local expression in the time domain. This is one interest of the spectral method which allows one to model the internal damping in the plate with such a flexibility. Considering the damping ratio values for wooden plate given in Ref. 5 in the range [0–3 kHz] corresponding to our case, a linear law has been chosen, of the form

$$\alpha_n=(R_p+\eta_p\omega_n)/2. \tag{25}$$

One must now write a finite difference scheme for the time discretization of Eqs. (20c)–(20g). The crucial point is to propose a stable coupling between two radically different time-resolution techniques: a continuous one for the plate equation and a discrete one for the string and air equations. The scheme is chosen in order to obtain a discrete energy identity similar to Eq. (13). In addition, we look for a scheme in which almost all computations are explicit (i.e., without matrix inversion), in particular for the 3D part. These two reasons lead to computing the variables v_{s_h}, p_h, and λ_h at time $t^{n+(1/2)}$, while q_h and $\underline{\mathbf{v}}_{a_h}$ are computed at time t^n, and to discretize Eq. (20g) which is now differentiated in time. The following system is obtained:

$$\begin{aligned}
&M_h^s\frac{v_{s_h}^{n+(1/2)}-v_{s_h}^{n-(1/2)}}{\Delta t}-D_hq_h^n=f_{s_h}^n,\\
&M_h^q\frac{q_h^{n+1}-q_h^n}{\Delta t}+D_h^{\mathsf{T}}v_{s_h}^{n+(1/2)}-J_h^{\mathsf{T}}v_{p_h}^{n+(1/2)}=0,\\
&M_h^a\frac{\underline{\mathbf{v}}_{a_h}^{n+1}-\underline{\mathbf{v}}_{a_h}^n}{\Delta t}-G_hp_h^{n+(1/2)}-B_{\Gamma_h}^{\mathsf{T}}\lambda_h^{n+(1/2)}=0,\\
&M_h^{p_a}\frac{p_h^{n+(1/2)}-p_h^{n-(1/2)}}{\Delta t}+G_h\underline{\mathbf{v}}_{a_h}^n=0,\\
&B_{\omega_h}\frac{v_{p_h}^{n+(1/2)}-v_{p_h}^{n-(1/2)}}{\Delta t}-B_{\Gamma_h}\frac{\underline{\mathbf{v}}_{a_h}^{n+1}-\underline{\mathbf{v}}_{a_h}^{n-1}}{2\Delta t}=0.
\end{aligned} \tag{26}$$

The resolution of the linear system consisting of Eqs. (24) and (26) imposes, in particular, to invert the mass matrices M_h^s, M_h^q, M_h^a, and $M_h^{p_a}$. To avoid this inversion at each time step, these matrices are reduced to diagonal matrices using the mass-lumping technique [see Eq. (22)].

We seek for $(v_{s_h}^{n+(1/2)},q_h^{n+1},v_{p_h}^{n+(1/2)},\dot{v}_{p_h}^{n+(1/2)},\underline{\mathbf{v}}_{a_h}^{n+1},p_h^{n+(1/2)},\lambda_h^{n+(1/2)})$, with all other terms being known. It is easy to show that if $\lambda^{n+(1/2)}$ is known, the rest of the computation is entirely explicit. For the computation of $\lambda^{n+(1/2)}$, one has to invert the matrix C_λ, where

$$C_\lambda=\frac{2B_{\omega_h}}{\Delta t}\left[I+J_h\left(\frac{1-\cos(\sqrt{K_h}\Delta t)}{\sqrt{K_h}}\right)J_h^{\mathsf{T}}\right]^{-1}B_{\omega_h}^{\mathsf{T}}+\Delta tB_{\Gamma_h}(M_h^a)^{-1}B_{\Gamma_h}^{\mathsf{T}}. \tag{27}$$

C_λ is symmetric and positive without any condition on the time step. Furthermore, this matrix is definite, provided that the following compatibility between the mesh of $\mathcal{C}$ and the mesh of Γ is satisfied:

$$\frac{h_\lambda}{h_a}\geqslant\alpha, \tag{28}$$

where α is a constant. This compatibility condition, which is not demonstrated here, is a consequence of the consistency of the fictious domain method.[17] In practice, α is approximately equal to 1.1.

The stability of the scheme given by Eqs. (24)–(26) is guaranteed with the help of an energy identity similar to Eq. (13). The details of the proof are beyond the scope of this paper. This leads to the following conditions which have to be satisfied for ensuring the stability:

$$\text{(i)}\quad \sqrt{\frac{T}{\rho_s}}\frac{\Delta t}{h_c}\leqslant 1, \tag{29}$$

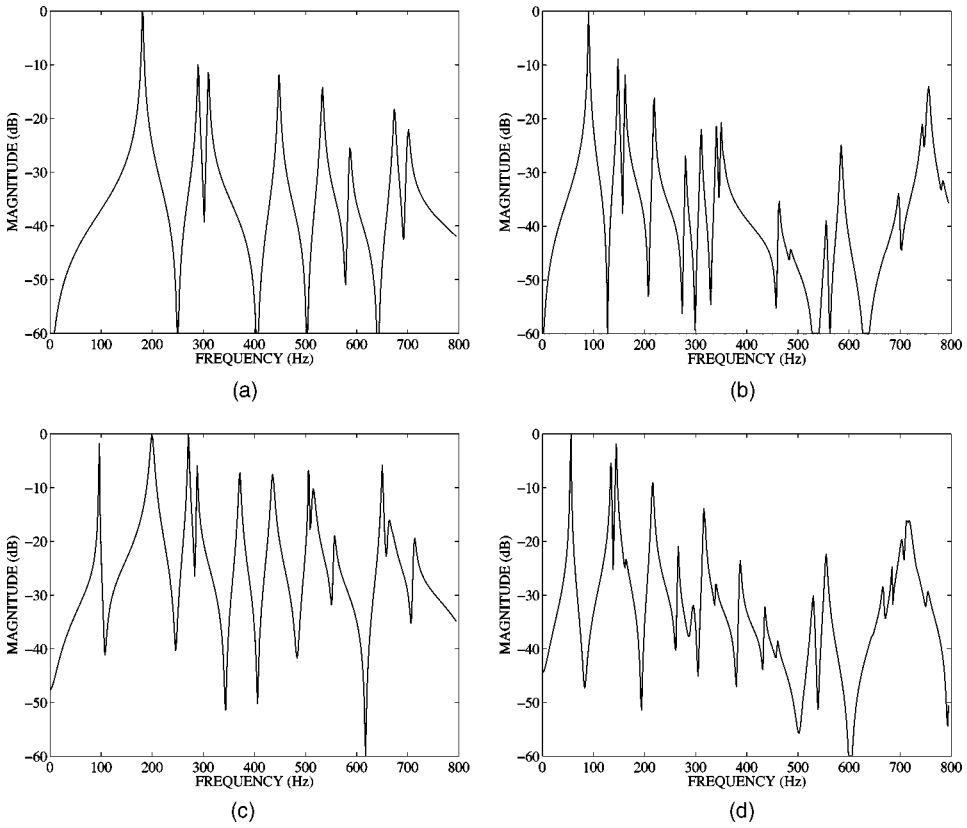

FIG. 7. Admittance curves at the bridge. A pulse force is applied to the lowest guitar string. The strings are damped. (a) Soundboard *in vacuo*, plate thickness 2.9 mm. (b) Soundboard *in vacuo*, plate thickness 1.45 mm. (c) Guitar coupled to the air, plate thickness 2.9 mm. (d) Guitar coupled to the air, plate thickness 1.45 mm.

$$\text{(ii)} \quad c_a \frac{\Delta t}{h_a} \leqslant \frac{1}{\sqrt{3}}.$$

One should notice that these two conditions are optimal, in the sense that they are identical to the usual stability conditions obtained for the standard finite difference discretization of the uncoupled 1D and 3D wave equation. This result shows the robustness of the coupling scheme.

The numerical parameters chosen for the numerical simulations presented in the following section and which fulfill the conditions Eqs. (28) and (29) are given in Table I.

IV. PRELIMINARY RESULTS AND DISCUSSION

The prime and most visible interest of our model is the computation of the complete 3D sound field radiated by the guitar (see Fig. 15). However, it is also necessary to validate our method through comparisons with existing results of the literature on guitars. In what follows, we start by presenting simulation results in terms of admittance, a quantity which is widely used for characterizing the essential coupling properties between strings and plate loaded by air in stringed instruments. In addition to the validation purpose, the specific interest of the presented results on admittances is to show the possible use of our model for comparing two different soundboards mounted on the same instrument. In our example, only the thickness is changed, all other parameters remaining identical. Such a modification would certainly be hard to realize on a real instrument. Finally, we show the differences, in terms of admittance and decay times, for a guitar body *in vacuo* compared to a guitar body in air. This clearly shows the various effects of both radiation and cavity field on the soundboard vibration.

Another interest of our model is the use of a variational formulation from which energetic quantities can be very easily derived. We use that property for gaining important information on the energy balance between strings, soundboard, and air.

The simulated sound pressure is observed in the time domain. Comparisons are made for two different values of box height and plate thickness, all other material and geometrical parameters remaining unchanged. The results show a clear difference between the waveforms. A spectral analysis is performed on the initial part of these simulated sounds. This analysis shows the role of both the string–body and air–body coupling in the spectral content and decay pattern of a guitar sound.

Finally, the spatial properties of the sound field are displayed in terms of instantaneous directivity patterns.

A. Admittance at the bridge

The admittance is defined as the ratio between velocity and force. In order to compute such a quantity, we use our model to simulate the velocity waveform consecutive to a force impulse $f(x,y,t)$ at one particular point at the bridge. In practice, the strings are damped and we use $f(x,y,t) = h(t)\delta_{x_0,y_0}(x,y)$, where $h(t)$ is given in Table I with $t_1 = t_2 = 5 \cdot 10^{-3}$ s. The selected point (x_0,y_0) corresponds to the attachment point of the lowest guitar string (6th string, note E_2). Using standard FFT tools, the admittance is simply

TABLE II. Analysis of simulated guitar sound pressure note E_2 (open 6th string) Damping factors and frequencies. The string partials are in bold. (a) Reference (plate thickness 2.9 mm, cavity height 10.4 cm). (b) Large cavity (plate thickness 2.9 mm, cavity height 21 cm). (c) Thin plate (plate thickness 1.45 mm, cavity height 10.4 cm).

(a) Reference		(b) Large cavity		(c) Thin plate	
F (Hz)	α (s^{-1})	F (Hz)	α (s^{-1})	F (Hz)	α (s^{-1})
82.4	**0.4**	76.7	1.6	55.5	1.6
96.6	2.1	**82.6**	**0.4**	**82.6**	**0.4**
164.7	**0.6**	**164.2**	**1.0**	135.0	4.8
200.6	20.8	183.3	14.9	144.4	6.5
247.8	**0.8**	**247.8**	**0.7**	**163.0**	**11.2**
272.3	7.9	274.7	8.3	166.4	1.7
289.0	7.0	293.0	7.7	216.4	11.9
330.6	**0.7**	**330.6**	**0.7**	**248.4**	**1.0**
372.9	12.9	355.6	7.2	266.7	7.4
413.0	**0.9**	**412.9**	**0.9**	296.1	30.0
437.6	19.0	436.2	15.0	317.0	8.7
495.6	**1.3**	**495.5**	**1.4**	319.0	8.3
508.7	1.6	505.6	1.1	**331.3**	**1.0**
517.1	21.9	515.0	19.7	340.4	8.7
558.3	15.6	**578.6**	**1.1**	388.5	12.0
578.5	**1.1**	656.5	11.4	**413.4**	**0.9**
652.7	9.3	**662.0**	**4.0**	436.6	9.7
661.1	**3.1**	672.1	24.4	461.6	12.4
672.7	26.7	707.4	7.6	**495.8**	**1.0**
716.0	13.0	**743.7**	**1.4**	531.2	8.2
743.7	**1.5**			**532.3**	**20.4**
				557.4	15.7
				578.6	**1.1**
				648.8	16.1
				660.6	**1.6**
				670.4	13.7
				693.4	39.4
				708.6	23.1
				720.5	29.1
				735.2	23.1
				744.4	**2.4**

obtained from the computation of the frequency response between velocity and force.

In order to illustrate the capabilities of our model, Fig. 7 shows typical results obtained in four different situations. The case (a) corresponds to the reference guitar "*in vacuo*." The reference guitar has a soundboard of thickness equal to 2.9 mm and a cavity height of 10.4 cm. In Fig. 7(b), the thickness is equal to 1.45 mm, all other parameters of the guitar remaining unchanged. Figures 7(c) and (d) correspond to the same configurations as (a) and (b), respectively, when the guitar vibrates in air.

As expected, the modal density is higher for case (b) than for case (a), and all frequencies are lowered (see also Table II). Figure 7(c) clearly shows additional peaks in the admittance curve, variation of the bandwidth for some peaks, and slight variations of the peak frequencies, compared to case (a). These phenomena are due to the coupling of the soundboard with cavity and external air. The frequency change of the two lowest peaks, in particular, follow the well-known rule[18]

$$f_+^2 + f_-^2 = f_1^2 + f_2^2, \tag{30}$$

where f_+ and f_- are the two lowest frequencies of the coupled system, whereas f_1 is the lowest acoustic eigenfrequency of the rigid cavity and f_2 is the lowest structural eigenfrequency of the soundboard. Here, we have $f_+ = 200.6$ Hz, $f_- = 96.6$ Hz, $f_1 = 117$ Hz, and $f_2 = 181.9$ Hz, which means that Eq. (30) is verified to within $\pm 5\%$. This discrepancy is mainly due to the fact that we do not have here an isolated system with two degrees of freedom, but a truncated system extracted from a continuous system. Frequency f_2 is obtained from the simulation of the complete guitar "*in vacuo*" (see Table II). Frequency f_1, like the other acoustic modes of the uncoupled system, is obtained from the simulation of the guitar coupled with external air and cavity while keeping the top plate rigidly fixed. Frequencies f_+ and f_- are derived from a spectral analysis performed either on the pressure or on the plate vibration, for the complete guitar.

The other lowest frequencies of the uncoupled acoustic modes are: 355, 699, 905, and 1046 Hz. It is interesting to notice that Eq. (30) also applies to other subsets of modes, provided that these subsets are reasonably well separated from the other modes. For the reference guitar, the coupled (called structural–acoustic or SA) modes at 373 and 437.6 Hz, for example, are due to the coupling between the acoustic mode at 355 Hz and the structural mode at 450 Hz.

Similar conclusions can be drawn from the comparison between Figs. 7(b) and (d), corresponding to the thin plate, with stronger variations of frequencies due to coupling in case (d) compared to case (c). In this latter case, notice that the modal density of the fluid–structure coupled system is high so that the maxima of the admittance curve cannot be well separated. This property also appears in case (b), though for higher frequencies than for case (d).

Finally, one should highlight the fact that the model yields admittance curves up to 3 kHz, as shown in Fig. 8. This is an improvement compared to previously published results on simulated guitars which are generally limited to less than 1 kHz.[19] These figures show, among other things, that the average slope for the mobility of the thin plate is relatively higher than the one of the reference soundboard. This suggests that the guitar with the thin soundboard is relatively more efficient in low frequencies compared to the high-frequency domain.

Detailed analysis of the simulated plate velocity at the junction between string and bridge, using the matrix-pencil method,[20] yields accurate values of the damping factors. Figures 9(a) and (b) show the effect of air loading and cavity on these factors for the soundboard vibration. For clarity, only the lowest modes, between 0 and 800 Hz, are presented. In this bandwidth, the admittance [Fig. 7(a)] shows 8 structural modes (*in vacuo* modes) from 182 Hz (1,1)-mode to 704 Hz (1,4)-mode. For these modes, the damping factors α (in s^{-1}) are only due to the material losses, which are assumed here to increase linearly with frequency [see Eq. (25)].

For the plate coupled with air [case 7(c)], 12 structural–acoustic modes (SA modes) were found. At this stage, notice that the matrix-pencil method yields accurate values of the eigenfrequencies and damping factors for the *in vacuo* soundboard, which validates the analysis. The damping factors for the air–body system are compared to those obtained from the analysis of the plate admittance *in vacuo*. These

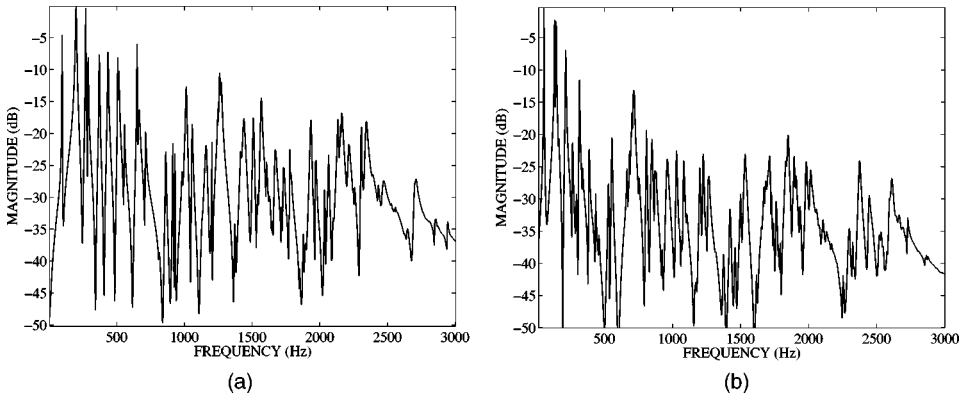

FIG. 8. Admittance curve at the bridge, in the interval [0–3000] Hz. (a) Reference guitar in air. (b) Guitar with thin plate in air.

factors are proportional to the sound power radiated by the instrument: high values of the damping coefficients correspond to strongly radiating modes.[21] For the reference case presented here, it can be seen, for example, that the SA modes at 201, 438, 517, and 673 Hz are efficient radiators.

For the reference guitar, it turns out that the Q-values, related to the damping factors α by the relation $Q=\pi f/\alpha$, are slightly higher in our simulation than those observed experimentally in real guitars (30–130 compared to 20–80), for the SA modes.[22] This should incite us to slightly increase the plate damping in future simulations in order to obtain sounds closer to real guitar sounds. Also, the fluid damping and the visco-thermal losses at the boundaries are not taken into account in our simulations. As a consequence, the simulated Q-values of some SA modes are high compared to real guitars, as it can be observed, for example, on the lowest structural–acoustic mode at 96.6 Hz.

In conclusion, the admittance analysis shows that, despite some crude aspects of the modeling (bracing, rigid back, air damping), our system is able to reproduce the main properties of a real guitar. In addition, the separate modeling of structural, acoustics, and structural–acoustic modes, respectively, not only validates the fictitious domain method, but also yields a powerful tool for the estimation and prediction of changes in radiated sound power consecutive to structural modifications of the instrument.

B. Energy exchange

Figure 10 shows the evolution of various energy quantities vs time for the plucked open string E_2 (fundamental 82.6 Hz).

As the string is in contact with the finger, most of the mechanical energy due to the plucking is transferred to the string. During this period of time, only a small amount of energy is transformed into quasistatic deformation of the plate and motion of the air. As the finger leaves the string, both plate and air energy increase almost instantaneously. The air-energy history is then dominated by almost periodic exchange with fundamental frequency equal to the fundamental frequency of the string. The plate-energy history is also periodic with the same fundamental frequency. For the case presented here, plate and air vibrations are in antiphase. The plate-energy history is also characterized by a modulation at a frequency nearly equal to the 5th harmonic of the fundamental. This property is due to the fact that the 5th harmonic of the string (around 413 Hz) is strongly coupled to an efficiently radiating structural–acoustic mode at 438 Hz.

After the pluck, the average magnitude of both plate and air energies corresponds approximately to 1 percent of the string energy. This proportion varies of course with the coupling properties between string and plate, and with the radiation efficiency of the instrument. However, the figure shown here corresponds to a typical order of magnitude for the lowest open string of a guitar, and this explains why guitar notes usual last for several seconds. As shown in Fig. 11, simulations made with the thickness of the top plate reduced by a factor of 2, all other parameters remaining unchanged, show a significant increase in the radiated sound power. In this case the average value of the air energy is equal to 10% of the string energy. As a consequence, the string vibrations are damped more rapidly.

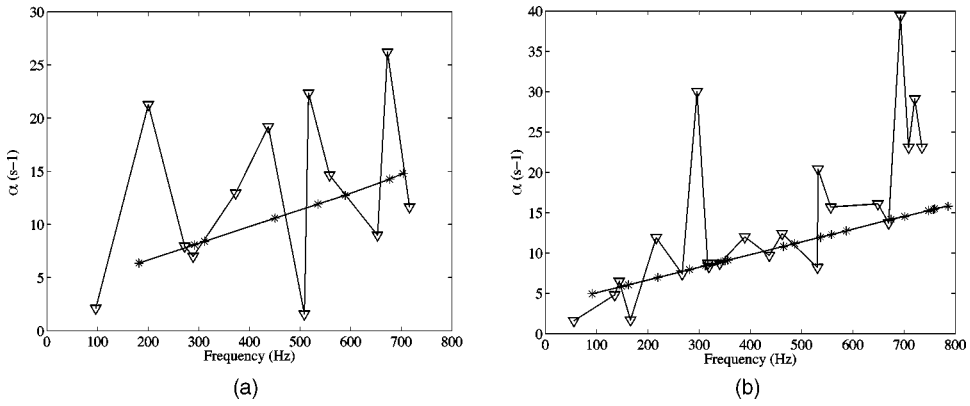

FIG. 9. Damping coefficients α (s^{-1}) for the lowest modes of the plate–air system (0–800 Hz). Comparison between structural and structural–acoustic modes. (a) Plate thickness 2.9 mm. Structural modes (*); structural–acoustic modes (∇). (b) Plate thickness 1.45 mm. Structural modes (*); structural–acoustic modes (∇).

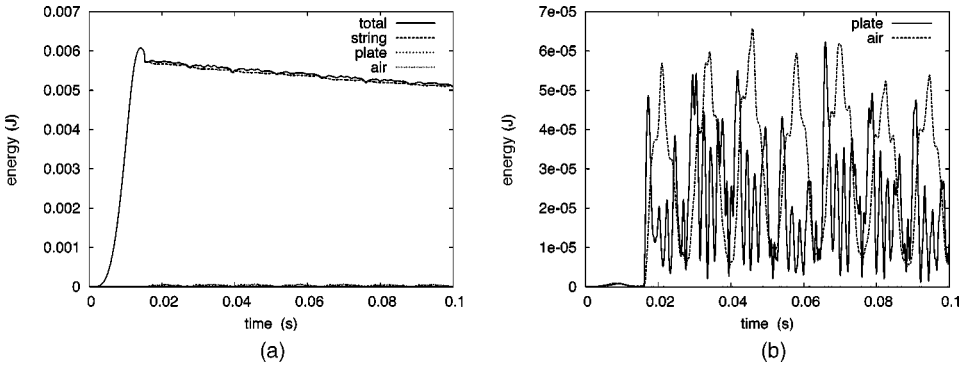

FIG. 10. (a) Evolution of the energy of string, plate, air, and total energy vs time for the plucked open string E_2 (fundamental 82.6 Hz) during the first 100 ms of the tone. Reference guitar. (b) Plate and air energy represented with appropriate scale.

C. The sound of the guitar in time

Examples of guitar pressure waveforms are simulated in three different situations, for a pluck on the open E_2 (6th) string. The first waveform shown in Fig. 12(a) corresponds to the reference guitar (see Table I). The waveform shown in Fig. 12(b) is obtained for a doubling of the cavity height, all other parameters remaining unchanged. Finally, the waveform shown in Fig. 12(c) corresponds to a top plate with thickness divided by a factor of 2, compared to the reference case, all other parameters remaining unchanged. For these three simulations, the tone duration is equal to 3 s. The pressure is simulated at a specific point in free space whose coordinates are $x=40$ cm, $y=5$ cm, and $z=60$ cm (see Fig. 1 for the definition of the axes).

The waveforms look clearly different. An accurate frequency analysis of these waveforms has been carried out with the help of the matrix-pencil method.[20] This analysis yields the frequencies and damping factors shown in Table II.

As expected, the pressure spectra are composed of string modes and of the SA modes of the guitar body coupled with air. All three spectra exhibit the nine lowest string modes and a variable number of SA modes, between 0 and 800 Hz. It can be seen that the coupling does not affect the frequencies and damping factors of the string modes significantly. As expected, the reference spectrum shows, in addition, the 12 SA modes observed in the admittance analysis. The damping factors of these modes are all significantly higher than those of the string modes, so that the well-known ''box sound'' in the guitar transient is damped more rapidly than the string components. The spectrum corresponding to the simulation with a large cavity shows 11 SA modes, in the same frequency range. Due to the doubling of the height some SA modes are strongly modified (such as the lowest one at 96.6 Hz, which becomes equal to 76.7 Hz). Other SA modes, which are mainly imposed by the lateral dimensions of the cavity, remain almost unchanged (272.3 and 289 Hz). For the simulated guitar sound with a thin plate, the pressure spectrum shows 22 SA modes between 0 and 800 Hz. This is, again, a result in accordance with the admittance analysis. As a consequence of the air–plate coupling, the lowest SA mode, in particular, is significantly reduced (55.5 Hz), compared to the reference case (96.6 Hz).

Figures 13 and 14 are aimed at summarizing the effects of the various coupling in the guitar through careful examination of the damping factors of the string's partials. Compared to Fig. 9, which illustrated the air–body coupling only, these data show that the sound of the guitar is governed by the combination of both air–body and string–body coupling.

The solid line in Fig. 13 shows the frequency-dependent damping on the isolated string: the quadratic function is a consequence of the damping model used (see Sec. II). The coupling of the string with the plate *in vacuo* (dashed line) contributes to increase its damping factors, with a more pronounced effect for the 2nd, 4th, 7th, and 8th partials, for which the degree of coupling with the plate modes is higher than for the other partials. The coupling of the plate with air modifies these factors substantially. In general, the damping factors increase due to radiation into the free space. However, since the air coupling also modifies the plate's modes, this can in turn modify the string–plate coupling and thus lead to a decrease of the damping factors for some string's components. Figure 13 shows that it is the case here for the 2nd, 4th, and 7th partials of the note E_2 (open 6th string) coupled to the reference guitar. Similarly, Fig. 14 shows the effect of reducing the plate thickness on the radiation of the

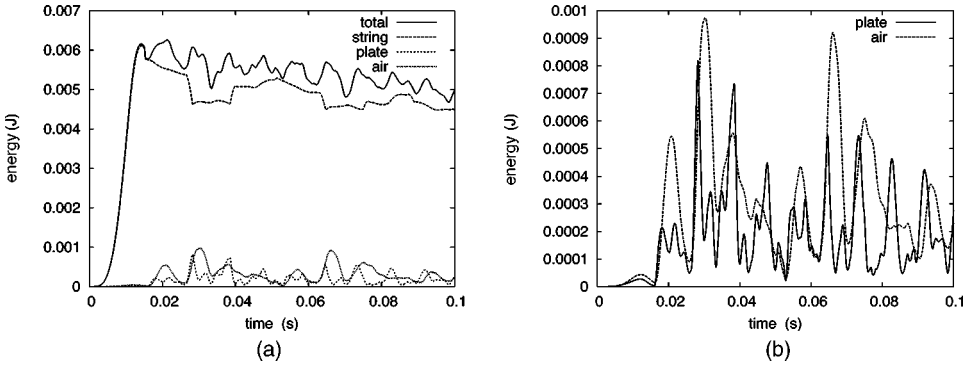

FIG. 11. (a) Evolution of the energy of string, plate, air, and total energy vs time for a plucked open string E_2 (fundamental 82.6 Hz) during the first 100 ms of the tone. Soundboard thickness 1.45 mm. (b) Plate and air energy represented with appropriate scale.

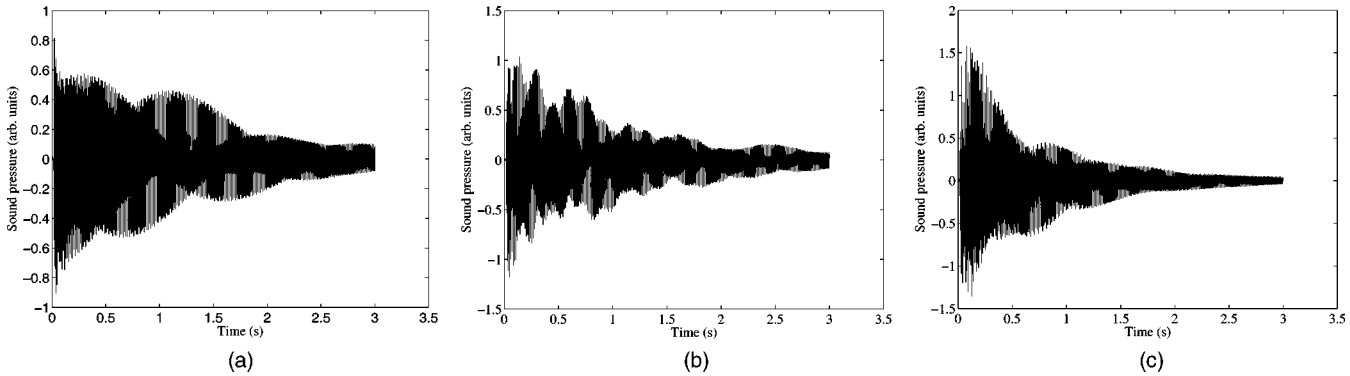

FIG. 12. Waveforms of the pressure recorded at the point ($x=40$ cm, $y=5$ cm, $z=60$ cm) (see Fig. 1 for the definition of the axes). (a) Reference (plate thickness 2.9 mm, cavity height 10.4 cm). (b) Large cavity (plate thickness 2.9 mm, cavity height 21 cm). (c) Thin plate (plate thickness 1.45 mm, cavity height 10.4 cm).

string's components. In the frequency range under examination, it can be seen that the thin plate is more efficient for allowing the guitar to radiate below 400 Hz, whereas the reference plate is more efficient between 400 and 800 Hz. In the low-frequency range, this result is due to the fact that the fluid–structure coupling is more pronounced for the thin plate than for the reference plate. However, as the frequency increases, it becomes hazardous to find a general interpretation for the changes in damping, since the values of the factors depend on the particular degrees of coupling between the string's modes and SA modes. A small change of thickness may alter this coupling substantially, as is experienced daily by guitar makers. More work is needed here for summarizing the efficiency of the instrument in the medium range, and in attempting to express the result in terms of global radiated power.

D. The sound of the guitar in space

Figure 15 shows an example of the spatial distribution of sound pressure in a plane perpendicular to the guitar, in the direction of the strings. For obvious reasons, only a small number of pictures which ''sample'' the acoustic field with a rather large period of time (typically a few milliseconds), can be inserted in this paper. The temporal evolution described below is better seen on a videotape and/or in animated pictures.[23]

The selected pictures are aimed at illustrating some of the basic physical phenomena relative to the acoustic field generated by a guitar, during the first 45 ms of the sound. For this reason, the time interval between consecutive pictures is not imposed to be kept constant. The black color corresponds to a negative acoustic pressure, whereas the white color corresponds to a positive pressure (see the scale). Figure 15(a) (at time 16.4 ms) shows the acoustic field right after the release of the string: two waves of opposite signs propagate inside and outside the cavity, respectively. At time 18.4 ms [Fig. 15(b)], the cavity is filled with a strong, positive pressure field. Plate and rose contributions are in phase, which yields a rather omnidirectional and homogeneous field in front of the instrument. At time 19.2 ms, Fig. 15(c) shows an example where the cavity field is not homogeneous. The external field is not symmetrical, which is a consequence of the fact that the various radiating components of the instruments are no longer in phase. Figure 15(d) (at time 21.1 ms) shows the opposite situation compared to case (b): the internal field is negative, like the near field of the instrument which shows

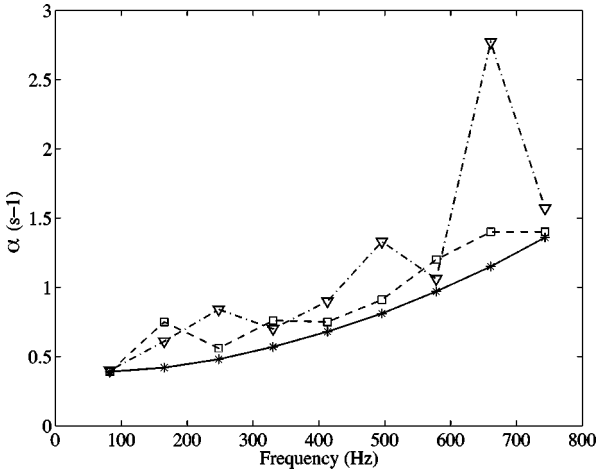

FIG. 13. Damping factors of the string partials. (*———) uncoupled string, (□---) string coupled to the soundboard, (▽-·-) string coupled to soundboard and air.

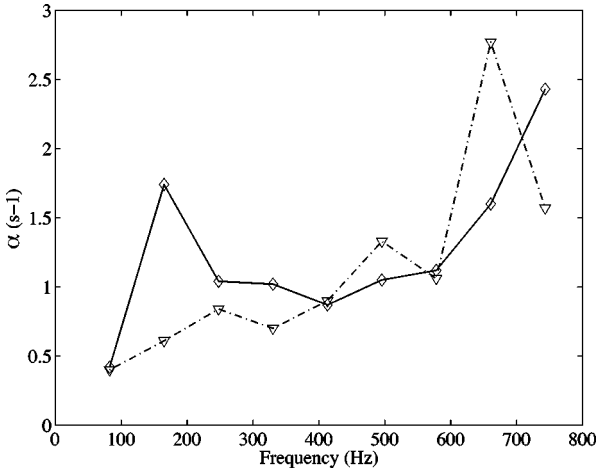

FIG. 14. Damping factors of the string partials coupled to soundboard and air (▽-·-) string coupled to the reference soundboard (plate thickness 2.9 mm), (◇———) string coupled to the thin soundboard (plate thickness 1.45 mm).

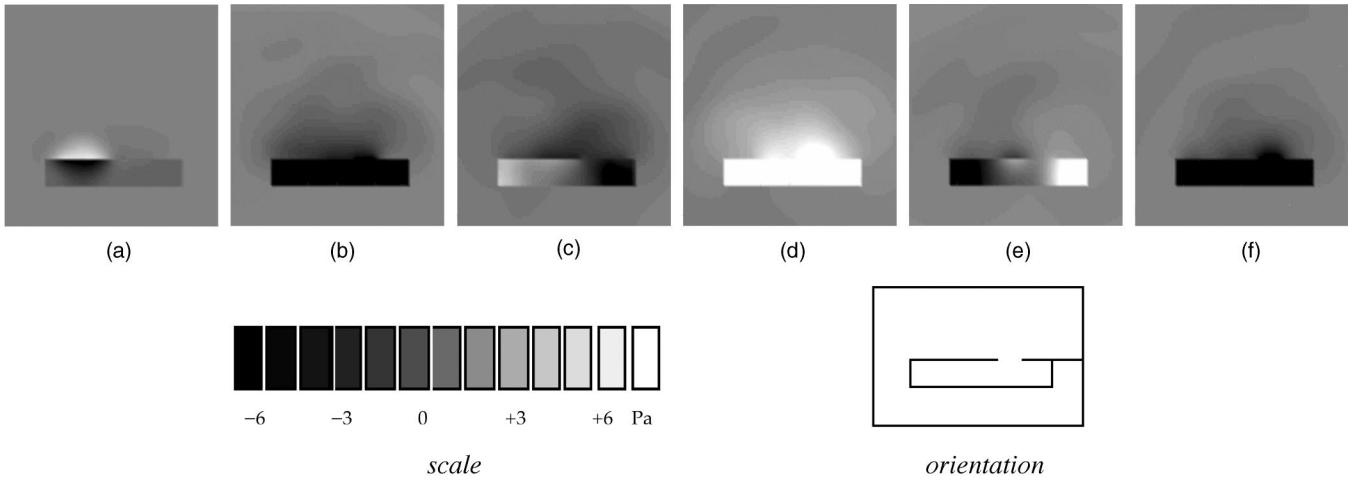

FIG. 15. Sound field radiated by the guitar in the plane $y=0$ for a plucked open string E_2 (fundamental 82.6 Hz) during the 45 first ms. Linear scale (Pa). (a) 16.4 ms. (b) 18.4 ms. (c) 19.2 ms. (d) 21.1 ms. (e) 23.1 ms. (f) 23.9 ms.

again a rather omnidirectional pattern. Similarly, Fig. 15(e) (at time 23.1 ms) shows the situation comparable to case (c), though with opposite signs. This leads to strong heterogeneities both in the internal and external field. The phenomena repeat themselves first pseudoperiodically during the transient where the ''box sound'' is present, and then become progressively periodic. It can be seen, for example, that case (f) (at time 23.9 ms) is comparable to case (b). Animated pictures[23] show, in addition, the propagation of the acoustic waves along the boundaries of the instruments. As a consequence, the acoustic load on the structure varies continuously with time.

The previous results suggest that the directivity of the instrument is not a stationary pattern. This feature is better shown on a logarithmic scale, as seen in Fig. 16, which represents instantaneous directivity patterns. The acoustic pressure is represented in decibels (dB). At time t the following function is plotted: $20\log_{10}|p(x,t)|/p_e$, where $p_e=2\cdot10^{-5}$ Pa is the reference. This figure has the property of enhancing the contributions of the various parts of the instruments to the radiated field while reducing the local differences in pressure, compared to the linear plot. The black color corresponds to 0 dB, while the white color corresponds to 120 dB (see the scale). Figure 16(a) (at time 9.6 ms) shows an example of almost-perfect omnidirectional pattern in front of the instrument. Figure 16(b) (at time 17.3 ms), on the contrary, denotes a multipolar radiation. In addition, the diffraction of the sound field on the back side of the guitar is clearly seen. Other examples of irregular directivity pattern can be also observed in Fig. 16(c) (at time 28.3 ms) and Fig. 16(d) (at time 32.4 ms), while Fig. 16(e) (at time 36.1 ms) shows again an almost constant directivity in the plane under study. In most of the cases, the sound field inside the cavity is significantly louder than the external field.

It could be of interest to validate the pressure patterns obtained with the present model with noncontacting TV-holography techniques, such as those developed by Runnemalm and Molin.[24] This should be done not only for stationary waves, but also for transients.

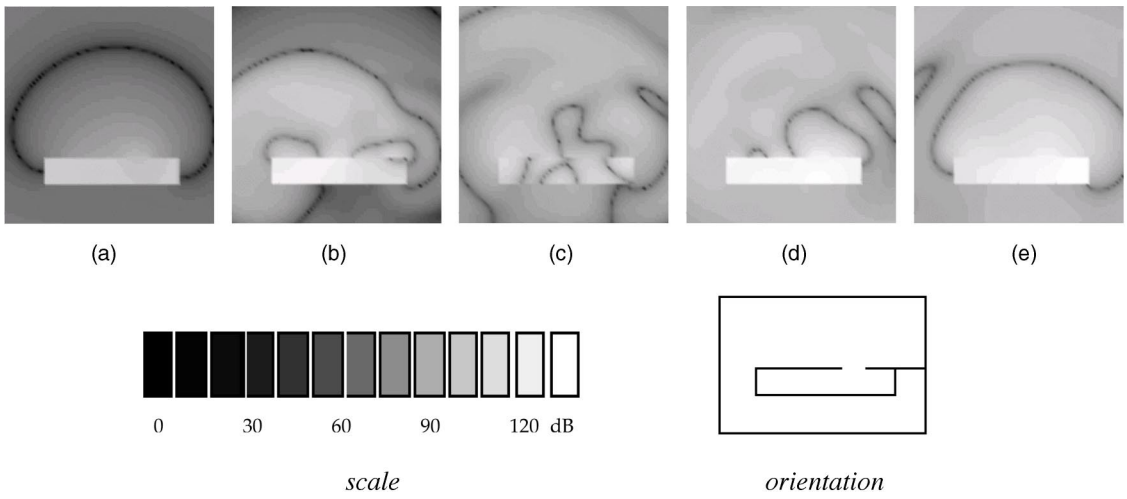

FIG. 16. Instantaneous directivity patterns: sound field radiated by the guitar in the plane $y=0$ for a plucked open string E_2 (fundamental 82.6 Hz) during the 45 first ms. dB scale. At time t, function $20\log_{10}|p(x,t)|/p_e$ is plotted where $p_e=2.10^{-5}$ Pa. (a) 9.6 ms. (b) 17.3 ms. (c) 28.3 ms. (d) 32.4 ms. (e) 36.1 ms.

V. CONCLUSION

The novel aspects of the present work arise from the demanding specificities of the model: complex geometry for the guitar, complex material for the top plate, coupling of the top plate with the partially opened cavity and the external free space. This relatively exhaustive model requires the association of highly elaborated numerical techniques in order to solve it with enough accuracy. The resolution has been made possible here through the use of a spectral method for the top plate, a fictitious domain method for the fluid–structure interaction problem and a conservative scheme for the time discretization. This method is applicable to other radiating structures composed of plates, holes, and cavities, and, in particular, to other stringed musical instruments.

Solving the vibroacoustical system in the time domain yields, among other things, the 3D temporal evolution of the acoustic field. From these results, important new features of the sound radiated by the guitar can be derived. The complexity and the variation in time of the directivity of the instrument, in particular, has been clearly shown.

The present method allows the separate computation of the acoustic modes, assuming a completely rigid body, of the structural modes, assuming that the instrument vibrates *in vacuo*, and of the coupled structural–acoustic modes for the complete air–structure model. This tool is thus applicable to, among other things, the evaluation of the relative contributions of structural losses and radiation losses in the sounds generated by the guitar. It is well-known that such a separation is hard to conduct experimentally.

In its present state, the guitar model is such that the effects of structural modifications on the produced sounds, such as plate thickness and cavity height, can be tested in a straightforward manner. Such simulations were systematically validated in this paper through analysis of admittance at the bridge, energy histories, and pressure signals. A good coherence was found between the results of this analysis, in terms of modal frequencies and damping factors. These results are compatible with experimental results published in the literature devoted to the acoustics of guitars. Because we have control here on the parameters fed into the model, it has been made possible to evaluate in detail the effects of the various sources of coupling (string–plate, plate–air) in terms of frequencies and decay rates.

Despite these interesting features, the present version of the model suffers from some numerical and physical limitations. As seen in Fig. 4, the main limitation due to numerical reasons is the bracing, which is rather crude compared to real guitars. This is due to the necessity of dealing with a more refined mesh if the purpose is to reproduce a real guitar adequately. From a physical point of view, the stronger limitation is probably due to the underestimation of the damping in the fluid, which might be mainly located at the rose and in the boundary layer in the box. More work is needed here for modeling and quantifying these effects convincingly. Other improvements should be investigated, such as the double polarization of the string and the vibrations of the neck. Although this part of the instrument does not participate directly in the radiation, its vibrations have effects on the motion of the other parts (strings, soundboard) to which it is coupled. This feature has been highlighted by Jansson.[25]

The present paper was mainly focused on the guitar model and on the numerical method to solve it, with only a few selected examples showing its capabilities in terms of guitar acoustics. At present, since the air equations are expressed in terms of pressure and acoustic velocity, it becomes possible to investigate other quantities of interest such as sound intensity and sound power. As an example, recent experimental work by Wang and Burroughs showed the interest of representing the complete acoustic intensity field around a stringed instrument in order to characterize its radiating properties.[26] With regard to such problems, the model developed here can be viewed as an interesting tool for validating the experiments theoretically.

APPENDIX A: THE KIRCHHOFF-LOVE'S PLATE EQUATION

1. Orthotropic plate equation

We present here the Kirchhoff–Love's plate equation in some particular Cartesian cases. $\underline{\underline{\mathcal{M}}}=a^3\mathbf{C}\underline{\underline{\varepsilon}}(\underline{\nabla} u_p)$ denotes the bending moment and $\mathbf{C}$ is the rigidity tensor for plates. One can write Eq. (5) in the following form (without damping terms):[7–10]

$$\underline{\underline{\mathcal{M}}}=\begin{pmatrix}\mathcal{M}_{xx}\\ \mathcal{M}_{yy}\\ \mathcal{M}_{xy},\end{pmatrix}=a^3\begin{pmatrix}D_1 & D_2/2 & 0\\ D_2/2 & D_3 & 0\\ 0 & 0 & D_4/2\end{pmatrix}\begin{pmatrix}\partial_{xx}u_p\\ \partial_{yy}u_p\\ \partial_{xy}u_p\end{pmatrix},$$

$$a\rho_p\frac{\partial^2 u_p}{\partial t^2}+\frac{\partial^2\mathcal{M}_{xx}}{\partial x^2}+\frac{\partial^2\mathcal{M}_{yy}}{\partial y^2}+2\frac{\partial^2\mathcal{M}_{xy}}{\partial x\partial y}$$
$$=\mathcal{F}-[p]_\omega \quad \text{in } \omega,$$

where D_1, D_2, D_3, and D_4, are the four rigidity constants of the plate.

2. Homogeneous isotropic plate equation

In the homogeneous isotropic case, one has: $D_1=D_3=(D_2/2+D_4/2)=E/[12(1-\nu^2)]$ where E and ν are the Young's modulus and Poisson's ratio, respectively. The Kirchhoff–Love's plate operator then becomes a usual bi-Laplacian. Equation (5) reduces to

$$a\rho_p\frac{\partial^2 u_p}{\partial t^2}+D_1a^3\left(1+\eta_p\frac{\partial}{\partial t}\right)\Delta^2 u_p+a\rho_pR_p\frac{\partial u_p}{\partial t}$$
$$=\mathcal{F}-[p]_\omega \quad \text{in } \omega.$$

3. Free-boundary condition

We give now the expression of the free-boundary conditions in the case of a plate with a straight edge. For example, if the y axis is a free boundary of the plate, the two conditions given by Eq. (7) can be written

$$\mathcal{M}_{xx}=0 \quad \text{and} \quad \frac{\partial\mathcal{M}_{xx}}{\partial x}+2\frac{\partial\mathcal{M}_{xy}}{\partial y}=0,$$
$$\text{along the edge } x=0.$$

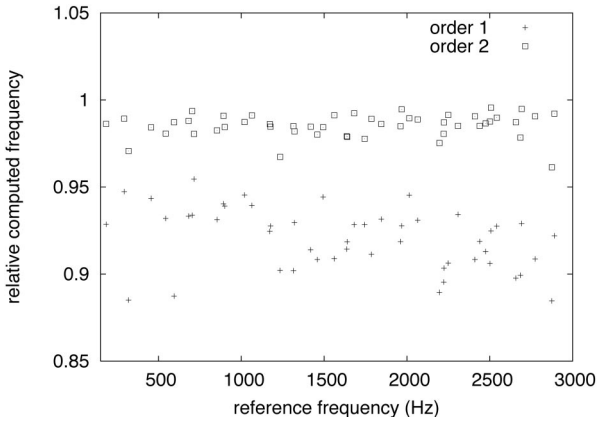

FIG. 17. Comparison between reference and computed eigenfrequencies of the soundboard. (×) relative frequency $f^1_{\text{com}}/f_{\text{ref}}$ computed using $P1$ finite elements. (□) relative frequency $f^1_{\text{com}}/f_{\text{ref}}$ computed using $P2$-alike finite elements.

APPENDIX B: DISPERSION ANALYSIS OF FINITE ELEMENT OF ORDER 1 AND 2 FOR THE PLATE

In order to show the interest of using of second-order finite element for the approximation of the plate equation, we compare here the values of the first 50 eigenfrequencies of the soundboard obtained using $P1$ or $P2$-alike continuous finite elements for the discretization of the variables v_p and $\underline{\underline{\mathcal{M}}}$, with the same computational effort.

Since the actual eigenvalues are not known analytically, references values denoted f_{ref} are first computed using a refined mesh of the soundboard with space step $h_p/2$ and using $P2$-alike continuous finite elements. The results are represented in Fig. 17. It appears immediately that the error made on the estimation of the eigenfrequencies is larger with the use of P_1 finite elements, since the error is greater than 5% for all frequencies. It is thus natural to choose second-order finite elements, which leads to a better approximation of the eigenfrequencies of the soundboard.

[1] L. Rhaouti, A. Chaigne, and P. Joly, "Time-domain simulation and numerical modeling of the kettledrum," J. Acoust. Soc. Am. **105**(6), 3545–3562 (1999).
[2] B. E. Richardson, "Numerical modelling of stringed musical instruments," in *SMAC 93* (Publication of the Royal Swedish Academy of Music, Stockholm, 1993), Vol. 79, pp. 457–462.
[3] A. Le Pichon, S. Berge, and A. Chaigne, "Comparison between experimental and predicted radiation of a guitar," Acustica **84**(1), 136–145 (1998).
[4] M. J. Elejabarrieta, A. Ezcurra, and C. Santamaria, "Coupled modes of the resonance box of the guitar," J. Acoust. Soc. Am. **111**(5), 2283–2292 (2002).
[5] A. Chaigne and C. Lambourg, "Time-domain simulation of damped impacted plates. I. Theory and experiments," J. Acoust. Soc. Am. **109**(4), 1422–1432 (2001).
[6] A. Chaigne, "On the use of finite differences for musical synthesis. Application to plucked string instruments," J. Acoust. **5**, 181–211 (1992).
[7] A. W. Leissa, *Vibrations of Plates* (NASA SP, Washington, D.C., 1969), Vol. 160.
[8] R. F. S. Hearmon, *An Introduction to Applied Anisotropic Elasticity* (Oxford University Press, London, 1961).
[9] S. Ambartsumyan, *Theory of Anisotropic Plates* (Technomic, Stanford, 1970).
[10] G. Caldersmith, "Vibration of orthotropic rectangular plates," Acustica **56**, 144–151 (1984).
[11] F. Millot, F. Collino, and P. Joly, "Fictitious domain method for unsteady problems: Application to electromagnetic scattering," *Mathematical and Numerical Aspects of Wave Propagation* (Mandelieu-La Napoule, 1995) (SIAM, Philadelphia, 1995), pp. 260–269.
[12] R. Glowinski, T. Pan, and J. Periaux, "A fictitious domain method for Dirichlet problem and applications," Comput. Methods Appl. Mech. Eng. **11**1(3–4), 283–304 (1994).
[13] G. Cohen, P. Joly, J. E. Roberts, and N. Tordjman, "Higher order triangular finite elements with mass lumping for the wave equation," SIAM (Soc. Ind. Appl. Math.) J. Numer. Anal. **38**(6), 2047–2078 (2001).
[14] F. Collino, "Conditions absorbantes d'ordre élevé pour des modèles de propagation d'onde dans des domaines rectangulaires," Technical Report No. 1790, INRIA, Rocquencourt.
[15] J. Nédélec, "Mixed finite elements in $\mathbb{R}^3$," Numer. Math. **35**, 315–341 (1980).
[16] E. Bécache, A. Chaigne, G. Derveaux, and P. Joly, "An explicit finite element scheme for time-dependent Kirchhoff–Love equations," in *Fifth International Conference on Mathematical and Numerical Aspects of Wave Propagation* (SIAM, Santiago, Spain, 2000), pp. 735–740.
[17] P. Joly and L. Rhaouti, "Domaines fictifs, éléments finis H(div) et condition de Neumann: Le problème de la condition inf-sup," C. R. Acad. Sci., Ser. I: Math. **328**(12), 1225–1230 (1999).
[18] O. Christensen and R. Vistisen, "A simple model for low-frequency guitar function," J. Acoust. Soc. Am. **68**, 758–766 (1980).
[19] B. Richardson, T. J. W. Hill, and S. Richardson, "Input admittance and sound field measurements of ten classical guitars," in *Proceedings of the Institute of Acoustics* (IOA, London, 2002), Vol. 24(2), pp. 1–10.
[20] J. Laroche, "The use of the matrix pencil method for the spectrum analysis of musical signals," J. Acoust. Soc. Am. **94**(4), 1958–1965 (1993).
[21] B. David and X. Boutillon, "Using vacuum to measure the acoustical efficiency," in *ISMA 95* (Société Francaise d'acoustique, Dourdan, France, 1995), pp. 380–385.
[22] B. E. Richardson, "Simple models as a basis for guitar design," Catgut Acoust. Soc. J. **4**(5), 30–36 (2002).
[23] E. Bécache, A. Chaigne, G. Derveaux, and P. Joly, "Numerical simulation of the acoustic guitar," DVD, VHS, and RealPlayer document, English, 2003, http://www.inria.fr/multimedia/Videotheque-fra.html
[24] A. Runnemalm and N.-E. Molin, "Operating deflexion shapes of the plates and standing aerial waves in a violin and a guitar model," Acustica **86**(5), 883–890 (2000).
[25] E. Jansson, *Acoustics for Violin and Guitar Makers* (Royal Institute of Technology, Stockholm, Stockholm, 2002).
[26] L. Wang and C. Burroughs, "Acoustic radiation from bowed violins," J. Acoust. Soc. Am. **110**(1), 543–555 (2001).